Adaptive Waveform Design in Rapidly-Varying Radar Scenes

Ying Li[†], William Moran[‡], Sandeep P. Sira[§], Antonia Papandreou-Suppappola[†], and Darryl Morrell[⋆]

[†]SenSIP Center, Dept. of Electrical Engineering, Arizona State University, Tempe, AZ
[‡]The University of Melbourne, Parkville, Vic 3010, Australia
[§]Zounds, Inc., Mesa, AZ
[⋆]Department of Engineering, Arizona State University, Polytechnic Campus, Mesa, AZ

Ying.Li.5@asu.edu, b.moran@ee.unimelb.edu.au, Sandeep.Sira@zoundshearing.com, papandreou@asu.edu, morrell@asu.edu

***Abstract*— We consider a waveform-agile sensing algorithm for designing transmitted waveforms in rapidly-varying radar scenes to improve target detection performance. Specifically, we first track the scattering function of rapidly-varying sea clutter in low signal-to-clutter ratios (SCRs) at each burst by estimating the clutter's space-time covariance matrix. Simultaneously, we schedule the waveform to be transmitted in the next burst by minimizing the sea clutter influence based on the estimated clutter statistics. The effectiveness of our waveform-agile sensing approach is demonstrated by detecting a moving target in heavy sea clutter using configured waveforms, and then comparing the resulting performance to that of detecting the target using fixed-parameter linear frequency-modulated waveforms.**

I. Introduction

Waveform diversity and design has recently been successfully used in radar applications, such as target detection and tracking, to improve radar performance. Increasing the accuracy of target detection and tracking can be of great importance in secure navigation, military and coastal security operations, and maritime rescue. As a result, waveform-agility can be pursued in real applications, especially with new developments in radar hardware and technologies that make it possible to design the transmitted waveform on-the-fly. When detecting or tracking a moving target in low SCR, waveform design becomes a challenging problem, especially for fast varying radar scenes. Although approaches to this problem under slowly-varying conditions have been proposed [1], [2], situations in which the radar scene varies quickly present significant additional difficulties.

In this work, we propose a waveform design method that adaptively chooses the parameters of the phase-modulated (PM) signal to be transmitted at the next time instant in order to minimize the effects of low SCR clutter in rapid-varying radar scenes. The method exploits a formulation of the space-time representation of the clutter scene in the scattering function domain. This formulation is vectorized to obtain a dynamic system characterization for detecting a target in heavy sea clutter. Our method first estimates the space-time covariance matrix of the sea clutter using the multiple particle filter sequential Monte Carlo method [3]. This method is chosen in order to overcome an inherent dimensionality problem. Then, an optimization procedure is used to find the PM waveform parameters that minimize the effect of the clutter and improve detection. The effectiveness of this method is demonstrated by detecting a moving target in a high sea clutter scenario.

The paper is organized as follows. In Section II, we describe the rapidly-varying radar scene and radar returns, and Section III provides the estimation method of the clutter space-time covariance matrix. In Section IV, we propose the waveform-agile algorithm for target detection in rapidly-varying clutter, and we provide simulations illustrating the performance of the algorithm in Section V.

II. Rapidly-varying radar scene characterization

In a rapidly-varying radar scene, we consider a radar operating at f_s Hz pulse repetition frequency (PRF) that transmits a burst of K pulses in each dwell, as shown in Figure 1. The length N_s pulse $s_n[i]$, $i = 0, 1, \ldots, N_s - 1$, is transmitted repeatedly K times throughout the nth dwell.

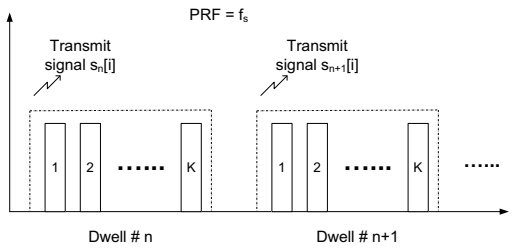

Fig. 1. Rapidly-varying radar scene transmitting K pulses in each dwell.

A. Scattering matrix

We consider the kth pulse, $k = 1, \ldots, K$, and the mth range bin, $m = m_0, m_1, \ldots, m_{M_n-1}$ at the nth dwell. Then, the corresponding complex reflectivity coefficients of the aggregate scatterers on the sea surface are denoted by $x_n[m, k]$. The coefficients form the reflectivity matrix B_n that is given

 9781-4244-2971-4/09/$25.00©2009 IEEE

by

$$B_n = \begin{bmatrix} x_n[m_0,1] & x_n[m_0,2] & \dots & x_n[m_0,K] \\ x_n[m_1,1] & x_n[m_1,2] & \dots & x_n[m_1,K] \\ \vdots & \vdots & \vdots & \vdots \\ x_n[m_{N_v-1},1] & x_n[m_{N_v-2},1] & \dots & x_n[m_{N_v-1},K] \end{bmatrix}$$

where m_0 is the lowest range bin in the validation gate at dwell n, and the validation gate at dwell n has M_n range bins. The reflectivity matrix has dimensions $N_v \times K$, where $N_v = M_n + N_s - 1$. The range (*fast time or delay*) increases down the columns, and the transmitted pulses (*slow time*) increase across the rows of B_n.

The scattering matrix A_n is defined with elements that are obtained by taking the short-time Fourier transform of the elements of B_n in the slow-time direction,

$$A_n[m,l] = \frac{1}{\sqrt{K}} \sum_{k=1}^{K} B_n[m,k] e^{-j2\pi kl/K}$$

where $l \in [-\frac{K-1}{2}, \cdots, \frac{K-1}{2}]$. Then,

$$A_n = B_n D \tag{1}$$

where D is the discrete Fourier transform matrix. Thus, A_n contains the range-Doppler description of the complex reflectivities in B_n.

The scattering matrix A_n provides the range-Doppler description of the scatterer complex reflectivities in matrix B_n. This is demonstrated in Figure 2. Each element in A_n describes the states of the scatterers. In each range bin, along the slow-time, static scatterers are represented in the middle column; the first $(K-1)/2$ elements represent the negative Doppler shifts and are related to the scatterers moving away from the sensor with different velocities; the last $(K-1)/2$ elements represent the positive Doppler shifts and are related to the scatterers moving toward the sensor with different velocities. According to the characteristics of sea clutter, most scatterers reside around the middle of each row (corresponding to zero Doppler).

B. Observation and dynamic models

In Figure 1, the return from each dwell is sampled at f_b Hz to yield $y_n[k,m] = y_n(k, mT_b)$, $k = 1, \dots, K$, $m = m_0, m_1, \dots, m_{M_n-1}$, where $T_b = 1/f_b$ is the *fast* sampling interval. Then, the radar return at the nth dwell is given by:

$$y_n[k,m] = \sum_{i=0}^{N_s-1} x_n[k, m-i] s_n[i] + v_n[k,m] \tag{2}$$

where $v_n[k,m]$ is additive white Gaussian noise. Note that we have assumed that an identical pulse $s_n[i], i = 0, 1, \cdots, N_s-1$ is transmitted throughout each dwell.

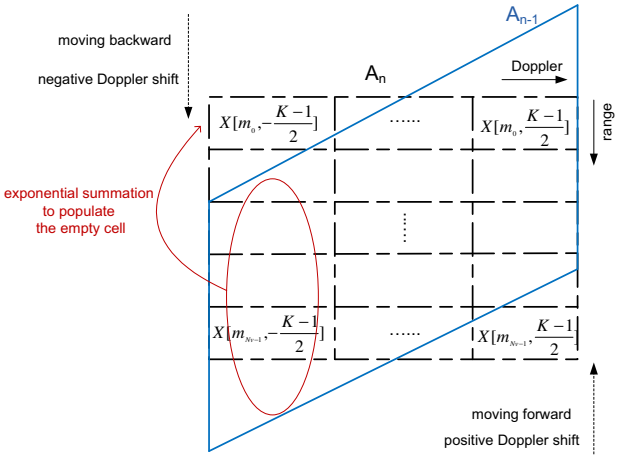

Fig. 2. Scattering matrix of sea clutter and the evolution of the scatterers.

The transmitted signal matrix P_n can be expressed as an $M_n \times N_v$ matrix given by

$$P_n = \begin{bmatrix} s_n[0] & s_n[1] & \cdots & s_n[N_s-1] & \cdots & 0 \\ 0 & s_n[0] & s_n[1] & \cdots & s_n[N_s-1] & \cdots \\ \vdots & \vdots & \vdots & \vdots & \cdots & \vdots \\ 0 & 0 & \cdots & \cdots & s_n[N_s-2] & s_n[N_s-1] \end{bmatrix}.$$

Then, using the transmitted signal matrix and the radar returns in (2), we can form the $M_n \times K$ observation matrix Y_n as

$$Y_n = P_n B_n + V_n \,. \tag{3}$$

Here, V_n is the $M_n \times K$ noise matrix at dwell n with elements $v_n[m,k]$.

We assume that the scatterers and the target move with constant velocity. As the scatterers move, some of them that do not stay in the middle columns of A_n will move out of the validation gate, and some range-Doppler cells will become empty. As shown in Figure 2, the solid parallelogram represents the scattering matrix at the $(n-1)$th dwell, and the dashed-dotted rectangular represents the scattering matrix at the $n$the dwell. The cells moving out of the matrix will be populated according to the adjacent elements in the same column (same Doppler shifts), which have constant velocity.

To better describe the evolution of the scattering matrix, an evolution matrix F is introduced, that describes the movement of the scatterers and the population of the empty cells. The new scatterer cells that are populated into the scattering matrix are described using exponential weighted summations of the complex reflectivities in the immediate neighborhood of these cells, as illustrated in Figure 2. This procedure will continue along each column until all empty cells are populated. We vectorize the matrix A_n to form $\mathbf{a}_n = \text{vec}(A_n)$ by stacking the columns of A_n from left to right to form a length KN_v vector. The evolution of the vectorized scattering matrix is given by

$$\mathbf{a}_n = F\mathbf{a}_{n-1} + \mathbf{w}_n \,. \tag{4}$$

The zero-mean, complex Gaussian noise $\mathbf{w}_n$ has covariance Q_n, and F incorporates the scatterer movements between dwells and populates the range-Doppler cells that move into the validation gate. The matrix F is a $KN_v \times KN_v$ block-diagonal matrix. When $l = -(K-1)/2, \ldots, -1$, the block matrix is given by

$$F_l = \begin{bmatrix} 2^{|l|-1}e^{-|l|\alpha} & \ldots & (2^{|l|-1} - |l| + 1)e^{-(N_v+|l|-1)\alpha} \\ \vdots & \vdots & \vdots \\ e^{-\alpha} & \ldots & e^{-N_v\alpha} \\ 1 & \ldots & 0 \\ 0 & \vdots & \vdots \\ \vdots & \ldots & 0 \end{bmatrix}.$$

When $l = 1, \ldots, (K-1)/2$, the block matrix is

$$F_l = \begin{bmatrix} 0 & \ldots & \vdots \\ \vdots & \vdots & 0 \\ 0 & \ldots & 1 \\ e^{-N_v\alpha} & \ldots & e^{-\alpha} \\ \vdots & \vdots & \vdots \\ (2^{l-1} - l + 1)e^{-(N_v+l-1)\alpha} & \ldots & 2^{l-1}e^{-l\alpha} \end{bmatrix},$$

and when $l = 0$, the scatterers are not moving, and the block matrix is an $N_v \times N_v$ identity matrix $\mathbb{I}_{N_v}$.

Based on the relationship between the reflectivity matrix B_n and the scattering matrix A_n in (1), the observation matrix Y_n in (3) can also be written as $Y_n = P_n A_n D^{-1} + V_n$. Using the matrix property $\text{vec}(GZL) = (L^H \otimes G)\,\mathbf{z}$, where G, Z, and L are three arbitrary matrices, $\mathbf{z} = \text{vec}(Z)$, and $\otimes$ denotes the Kronecker product [4], the vectorized observation is then given by

$$\begin{aligned} \mathbf{y}_n &= (D^{-H} \otimes P_n)\mathbf{a}_n + \mathbf{v}_n \\ &= \check{P}_n \mathbf{a}_n + \mathbf{v}_n \end{aligned} \quad (5)$$

where $\mathbf{y}_n = \text{vec}(Y_n)$, $\check{P}_n = D \otimes P_n$, and H denotes the Hermitian operator.

Thus, Equations (4) and (5) represent the dynamic state and observation equations in a state space representation where $\mathbf{a}_n$ is the unknown state. And, $\mathbf{a}_n$, the vectorized scattering matrix A_n, is related to the original reflectivity matrix B_n of the clutter using (1).

III. Estimation of sea clutter statistics

As we will see in Section IV, the waveform-agile detection algorithm highly depends on the accurate estimation of sea clutter statistics. In this section, we discuss the clutter estimation algorithm introduced in [5].

Let $\mathbf{\Sigma}_{\mathbf{a}_n}$ be the covariance matrix of $\mathbf{a}_n$. The dynamic model in (4) can also be described as:

$$\mathbf{\Sigma}_{\mathbf{a}_n} = \text{E}[\mathbf{a}_n \mathbf{a}_n^H] = F\mathbf{\Sigma}_{\mathbf{a}_{n-1}}F^H + Q_n, \quad (6)$$

where Q_n is the covariance matrix of $\mathbf{w}_n$. Similarly, the covariance matrix of the vectorized observations in (5) can be extended to:

$$\mathbf{\Sigma}_{\mathbf{y}_n} = \check{P}_n \mathbf{\Sigma}_{\mathbf{a}_n} \check{P}_n^H + R_n, \quad (7)$$

where R_n is the covariance matrix of $\mathbf{v}_n$. Using (7), we can obtain $p(\mathbf{y}_n|\mathbf{\Sigma}_{\mathbf{a}_n})$ to update the filter. Note that Q_n in (6) and R_n in (7) are assumed to be Wishart distributed; this follows from the covariance of the multinormal samples $\mathbf{w}_n$ and $\mathbf{v}_n$. Also, as A_n and B_n are related, once we estimate $\mathbf{\Sigma}_{\mathbf{a}_n}$, we can also obtain $\mathbf{\Sigma}_{\mathbf{b}_n} = (D \otimes \mathbb{I}_{N_v})\mathbf{\Sigma}_{\mathbf{a}_n}(D^H \otimes \mathbb{I}_{N_v})$.

Particle filtering (PF) is a sequential Monte Carlo method that uses sampling to approximate probability density functions. It provides a good approximation to Kalman filtering when the system models are nonlinear or non-Gaussian [6], [7]. However, when the dimensionality of the state space is large, as in our case, a huge set of particles is needed to provide sufficient support and the computational complexity becomes prohibitive. As discussed in [3], multiple particle filtering (MPF) can be used to overcome this dimensionality problem as follows. If the dynamic and measurement equations of a system can be written as $\boldsymbol{\alpha}_n = f_n(\boldsymbol{\alpha}_{n-1}, \boldsymbol{\omega}_{n-1})$ and $\boldsymbol{\beta}_n = h_n(\boldsymbol{\alpha}_n, \boldsymbol{\gamma}_n)$, where $\boldsymbol{\alpha}_n$ is a high-dimensional system state vector at time step n, f_n and h_n are (possibly nonlinear) functions, and $\boldsymbol{\omega}_n$ and $\boldsymbol{\gamma}_n$ are random vectors. Using the MPF approach in [3], $\boldsymbol{\alpha}_n$ is divided into L subvectors, given by $\boldsymbol{\alpha}_n = [\boldsymbol{\alpha}_{1,n}^T\ \boldsymbol{\alpha}_{2,n}^T\ \ldots\ \boldsymbol{\alpha}_{L,n}^T]^T$. Each $\boldsymbol{\alpha}_{l,n}$, $l = 1, 2, \ldots, L$, is estimated using a different PF. As a result, L PFs are running simultaneously, and the state vector $\boldsymbol{\alpha}_n$ is put together accordingly at each time n.

In order to take advantage of Bayesian techniques to solve the system equations, we vectorize the dynamic and observation models in (6) and (7). Specifically, we obtain

$$\begin{aligned} \tilde{\mathbf{\Sigma}}_{\mathbf{a}_n} &= (F \otimes F)\tilde{\mathbf{\Sigma}}_{\mathbf{a}_{n-1}} + \tilde{\mathbf{Q}}_n \\ \tilde{\mathbf{\Sigma}}_{\mathbf{y}_n} &= (\check{P}_n \otimes \check{P}_n)\tilde{\mathbf{\Sigma}}_{\mathbf{a}_n} + \tilde{\mathbf{R}}_n, \end{aligned} \quad (8)$$

where $\tilde{\mathbf{\Sigma}}_{\mathbf{a}_n} = \text{vec}(\mathbf{\Sigma}_{\mathbf{a}_n})$, $\tilde{\mathbf{\Sigma}}_{\mathbf{y}_n} = \text{vec}(\mathbf{\Sigma}_{\mathbf{y}_n})$, $\tilde{\mathbf{Q}}_n = \text{vec}(\mathbf{Q}_n)$ and $\tilde{\mathbf{R}}_n = \text{vec}(\mathbf{R}_n)$. After vectorization, the dimensionality of $\tilde{\mathbf{\Sigma}}_{\mathbf{a}_n}$ is given by $\Xi = (KN_v)^2$. The value of Ξ can be quite large, even if we consider a small number of pulses. For example, if we use $K = 9$ pulses and $M_n = 10$ range bins, then even if we reduce the signal length to $N_s = 6$, we obtain $N_v = M_n + N_s - 1 = 15$ and thus $\Xi = 18,225$. This implies that we need to estimate an unknown dynamic state whose dimensionality is 18,225; this high dimensionality prevents direct implementation of particle filtering or Kalman filtering, even if the transformations are linear. We therefore apply the MPF approach discussed above [3].

In (8), the evolution matrix $F \otimes F$ is block diagonal,

$$F \otimes F = \begin{bmatrix} F_1 \otimes F & 0 & \cdots & 0 \\ 0 & F_2 \otimes F & \cdots & 0 \\ & & \cdots & \\ 0 & 0 & \cdots & F_K \otimes F \end{bmatrix}$$

and F_k is defined in Section II. The structure of $F \otimes F$ leads to a natural decomposition of the dynamics of the state vector

into K independent subsystems,

$$\tilde{\mathbf{\Sigma}}_{\mathbf{a}_n} = \left[\begin{array}{cccc} \mathbf{\Lambda}_{1,n}^T & \mathbf{\Lambda}_{2,n}^T & \dots & \mathbf{\Lambda}_{K,n}^T \end{array} \right]^T$$

where each vector $\mathbf{\Lambda}_{k,n}$, $k = 1, \dots, K$, has dimension KN_v^2. As a result, we can use the MPF with $L = K$ PFs applied simultaneously, one for each of the K subsystems. For the kth subsystem, the estimation of this segment of the current state can be obtained using the dynamic and measurement models

$$\begin{aligned} \mathbf{\Lambda}_{k,n} &= (F_k \otimes F)\mathbf{\Lambda}_{k,n-1} + \mathbf{V}_{k,n} \\ \tilde{\mathbf{\Sigma}}_{\mathbf{y}_n} &= (\check{P}_n \otimes \check{P}_n)\tilde{\mathbf{\Sigma}}_{\mathbf{a}_n} + \tilde{\mathbf{R}}_n \,. \end{aligned}$$

For the kth PF, the weight of the ith particle, $i = 1, \dots, M_s$ can be updated according to

$$w_{k,n}^{(i)} \propto w_{k,n-1}^{(i)} \frac{p(\mathbf{\Sigma}_{\mathbf{y}_n} | \mathbf{\Lambda}_{k,n}^i \tilde{\mathbf{\Lambda}}_{-k,n}^{(i)}) p(\mathbf{\Lambda}_{k,n}^{(i)} | \mathbf{\Lambda}_{k,n-1}^{(i)} \hat{\mathbf{\Lambda}}_{-k,n-1})}{\pi_k(\mathbf{\Lambda}_{k,n}^{(i)} | \mathbf{\Lambda}_{k,n-1}^{(i)}, \hat{\mathbf{\Lambda}}_{-k,n-1}, \tilde{\mathbf{\Sigma}}_{\mathbf{y}_n})}$$

where $\tilde{\mathbf{\Lambda}}_{-k,n} = [\hat{\mathbf{\Lambda}}_{1,n}^T \ \cdots \ \hat{\mathbf{\Lambda}}_{k-1,n}^T \ \hat{\mathbf{\Lambda}}_{k+1,n}^T \ \cdots \ \hat{\mathbf{\Lambda}}_{k,n}^T]^T$, $\hat{\mathbf{\Lambda}}_{j,n}^T = \sum_{i=1}^{Ms} w_{j,n-1}^{(i)} \mathbf{\Lambda}_{j,n}^{(i)}$, $j \neq k$, and $\pi_k(\cdot)$ is the importance density that is chosen here to be the prior density [6]. The observation used in the kth PF has a complex Gaussian distribution with zero-mean and covariance matrix $\mathbf{\Sigma}_{\mathbf{y}_n}$.

IV. Waveform Design Algorithm

In order to improve the target detection performance in rapidly-varying radar scenes, we propose to design the transmit waveforms at each time instant. Specifically, instead of transmitting the same type of pulse at all dwells, the transmitted waveform is designed at each dwell to minimize a cost function in terms of the estimated clutter covariance matrix.

Figure 3 demonstrates the proposed waveform design algorithm. At the beginning of the algorithm, K pulses of a linear frequency-modulated (LFM) chirp with fixed parameters is transmitted at the first ($n = 1$) dwell. Using the observations and the method described in Section III, the covariance matrix ($\hat{\mathbf{\Sigma}}_{\mathbf{a}_n}$) of the fast-varying sea clutter is estimated. Using this estimate, we predict the covariance matrix for the next time step using (6). That is, we obtain $\bar{\mathbf{\Sigma}}_{\mathbf{a}_n} = F\hat{\mathbf{\Sigma}}_{\mathbf{a}_n}F^H$. We then design the next waveform to transmit by minimizing a cost function that is aimed to reduce the effect of the clutter. This waveform is then transmitted at the next time step, and the observations are used to estimate the clutter statistics at this new time step. The waveform design algorithm steps are also summarized in Table I.

The waveform we use in the design algorithm at each time step n is a unimodular PM waveform given by

$$s_n(t; \text{PM}) = \exp\left(j\boldsymbol{\psi}(t)\right), \quad 0 \leq t \leq T_d,$$

where the phase modulation can be expanded in terms of an orthogonal set of basis functions as $\boldsymbol{\psi}(t) = \sum_{i=1}^{N} \theta_i \psi_i(t)$, where

$$\psi_i(t) = \begin{cases} 1, & (i-1)\Delta T \leq t \leq i\Delta T \\ 0, & \text{otherwise} \end{cases} .$$

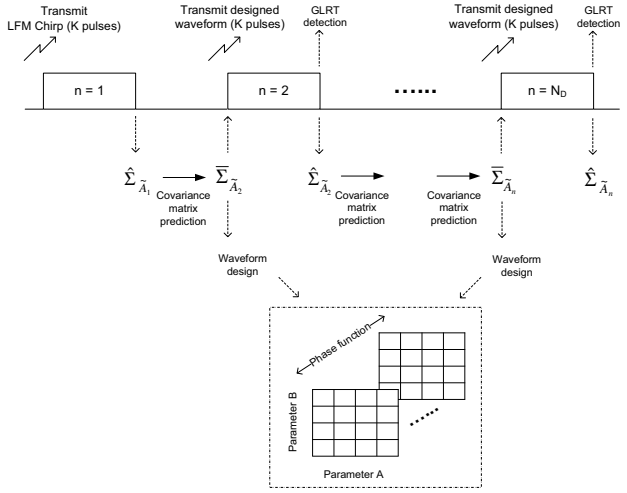

Fig. 3. Depiction of waveform design algorithm.

Here, T_d and ΔT are the pulse duration and sampling interval, respectively.

In order to mitigate the effect of the clutter, we choose the waveform at time step n that minimizes the cost function given by the trace of $\check{P}_n \bar{\mathbf{\Sigma}}_{\mathbf{a}_n} \check{P}_n^H$ [2], [8]. Recall that $\check{P}_n$ is related to the transmitted waveform matrix P_n in (3) and thus to the transmitted signal. Also, the covariance matrix $\mathbf{\Sigma}_{\mathbf{y}_n}$ of the vectorized observations in (5) is related to $\check{P}_n \mathbf{\Sigma}_{\mathbf{a}_n} \check{P}_n^H$ in (7), where $\mathbf{a}_n$ is the vectorized scattering matrix of the clutter. Thus, minimizing this covariance matrix results in minimizing the effect of the clutter on the target detection.

The waveform selection algorithm is thus given by

$$s_n^*(t; \text{PM}) = \arg \min_{s_n(t;\text{PM})} \text{trace}(\check{P}_n \bar{\mathbf{\Sigma}}_{\mathbf{a}_n} \check{P}_n^H) \tag{9}$$

where . Once the optimal waveform is transmitted, the target is detected using the generalized likelihood ratio test (GLRT) [9]. With respect to range bin j, let $\mathcal{H}_0$ denote the hypothesis that only clutter is present, and let $\mathcal{H}_1$ denote the presence of both clutter and target. The GLRT detector decides $\mathcal{H}_1$ if

$$\Lambda_j^{GLRT} = \ln \frac{p(\mathbf{y}_{n,j} | \mathcal{H}_1, \bar{\mathbf{\Sigma}}_{\mathbf{a}_n})}{p(\mathbf{y}_{n,j} | \mathcal{H}_0, \bar{\mathbf{\Sigma}}_{\mathbf{a}_n})} > \gamma, \tag{10}$$

where γ is a threshold that achieves a desired false alarm probability and can be calculated using (7).

V. Simulations

In our simulations, we compared the detection performance of a moving target in heavy sea clutter by transmitting fixed LFM chirps and designed PM waveforms under different SCR scenarios. We used $K = 9$ pulses to transmit in each dwell, and the validation gate size was $M_n = 11$. The length of the transmitted waveform transmitted was $N_s = 6$. For the MPF, we used $L = 9$ PFs, and each PF used 50 particles. The simulated sea clutter was generated using a compound-Gaussian model [10]; at each time step, 200 Monte Carlo simulations were used to obtain the space-time covariance matrix of the

TABLE I

WAVEFORM DESIGN ALGORITHM DESCRIPTION.

At time step $n = 1$,

- At the beginning of the dwell:
  - transmit K LFM chirp pulses with fixed parameters
- At the end of the dwell:
  - Estimate the sea clutter covariance matrix, $\hat{\mathbf{\Sigma}}_{\mathbf{a}_n}$

for $n = 2 : N_D$,

- Calculate the predicted covariance matrix, $\bar{\mathbf{\Sigma}}_{\mathbf{a}_n}$, based on the previous estimate using (6)
- Design the transmitted waveform by:

$$s_n^*(t;\text{PM}) = \arg \min_{s_n(t;\text{PM})} \text{trace}(\check{P}_n \bar{\mathbf{\Sigma}}_{\mathbf{a}_n} \check{P}_n^H)$$

- At the beginning of the dwell:
  - Transmit the designed waveform $s_n^*(t;\text{PM})$
- At the end of the dwell:
  - GLRT detection
  - Estimate the covariance matrix at this time step.

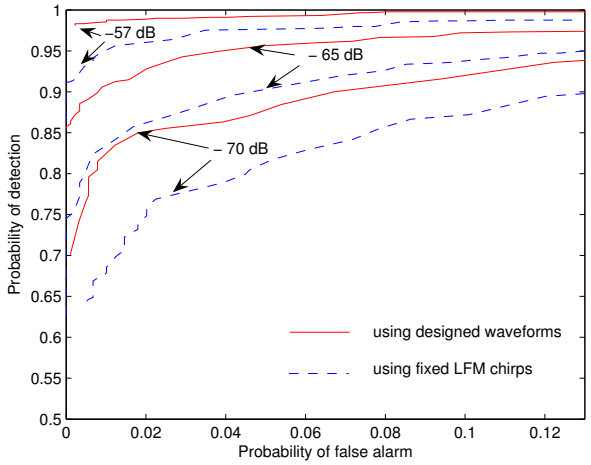

Fig. 4. Detection performances of the waveform design approach compared with using fixed waveforms under different SCR values.

reflectivity vector. The range bin size and Doppler resolution were chosen such that, from one dwell to another, the scatterer in the lth column, $l = -(K-1)/2, \cdots, 0, \cdots, (K-1)/2$, of the scattering function moved by l bins. The target was assumed to move with a known constant velocity of 20 m/s. Target returns from all pulses and range bins were combined to form the observation vector. The amplitudes of the target returns were sampled from a zero-mean, complex Gaussian process with known variance.

Based on the estimated space-time covariance matrix of the sea clutter using the MPF method, the GLRT detector was used to detect the range bin location of the target, utilizing each pulse of each burst. The PM waveforms transmitted at each dwell were designed by minimizing the cost function in (9) following Section IV. The receiver-operating characteristict (ROC) curves are shown in Figure 4 for 57 dB, -65 dB, and -70 dB SCR values. For comparison, the detection performance of fixed LFM chirp waveforms is also shown in Figure 4. These waveforms used a chirp rate of 1,000 GHz/s and time duration 1.2×10^{-12} s. As we can see, the waveform design approach increased the detection performance by about 5 dB.

VI. CONCLUSION

We proposed a waveform-agile target detection algorithm for the difficult scenarios of rapidly-varying radar scenes. We first estimated the space-time covariance matrix of the sea clutter using multiple particle filtering, and then we discussed the waveform design algorithm to adaptively design the transmitted signal at each time step. The proposed technique minimizes a cost function to reduce the influence of the clutter on detecting a moving target. We demonstrated the increased performance of our new approach using simulations and compared it with using fixed linear frequency-modulated waveforms.

REFERENCES

[1] B. Friedlander, "A subspace method for space time adaptive processing," *IEEE Transaction on Signal Processing*, vol. 53, pp. 74–82, January 2005.

[2] S. P. Sira, D. Cochran, A. Papandreou-Suppappola, D. Morrell, W. Moran, S. Howard, and R. Calderbank, "Adaptive waveform design for improved detection of low-RCS targets in heavy sea clutter," *IEEE Journal on Selected Topics in Signal Processing*, pp. 56–66, June 2007.

[3] P. M. Djuric, T. Lu, and M. F. Bugallo, "Multiple particle filering," in *IEEE International Conference on Acoustics, Speech, and Signal Processing*, June 2007, pp. 1181–1184.

[4] J. R. Magnus and H. Neudecker, Eds., *Matrix Differential Calculus with Applications in Statistics and Econometrics*. Wiley, 1999.

[5] Y. Li, S. P. Sira, B. Moran, S. Suvorova, D. Cochran, D. Morrell, and A. Papandreou-Suppappola, "Adaptive sensing of dynamic target state in heavy sea clutter,," in *IEEE Int. Workshop on Computational Advances in Multi-Sensor Adaptive Processing*, December 2007, pp. 9–12.

[6] A. Doucet, N. de Freitas, and N. J. Gordon, Eds., *Sequential Monte Carlo Methods in Practice*. Springer, 2001.

[7] M. S. Arulampalam, S. Maskell, N. Gordon, and T. Clapp, "A tutorial on particle filters for online nonlinear/non-Gaussian Bayesian tracking," *IEEE Transactions on Signal Processing*, vol. 50, pp. 174–188, 2002.

[8] S. Sira, D. Cochran, A. Papandreou-Suppapola, D. Morrell, W. Moran, and S. Howard, "A subspace-based approach to sea clutter suppression for improved target detection," in *Asilomar Conference on Signals, Systems, and Computers*, Pacific Grove, CA, October 2006, pp. 752–756.

[9] S. M. Kay, *Fundamentals of Statistical Signal Processing: Detection Theory*. Prentice-Hall, 1993, vol. 2.

[10] K. D. Ward, C. Baker, and S. Watts, "Maritime surveillance radar, Part I: Radar scattering from the ocean surface," *IEE Proc. F: Communications, Radar and Signal Processing*, vol. 137, no. 2, pp. 51–62, 1990.